ERDC/CRREL TR-22-7

US Army Corps of Engineers®
Engineer Research and Development Center

ERDC
ENGINEER RESEARCH & DEVELOPMENT CENTER

Engineering for Polar Operations, Logistics, and Research (EPOLAR)

South Pole Station Snowdrift Model

Luke Allen, Robert Haehnel, and Yonghu Wenren

August 2022

Cold Regions Research and Engineering Laboratory

The US Army Engineer Research and Development Center (ERDC) solves the nation's toughest engineering and environmental challenges. ERDC develops innovative solutions in civil and military engineering, geospatial sciences, water resources, and environmental sciences for the Army, the Department of Defense, civilian agencies, and our nation's public good. Find out more at www.erdc.usace.army.mil.

To search for other technical reports published by ERDC, visit the ERDC online library at https://erdclibrary.on.worldcat.org/discovery.

Engineering for Polar Operations, Logistics,
and Research (EPOLAR)

ERDC/CRREL TR-22-7
August 2022

South Pole Station Snowdrift Model

Luke Allen, Robert Haehnel, and Yonghu Wenren

US Army Engineer Research and Development Center (ERDC)
Cold Regions Research and Engineering Laboratory (CRREL)
72 Lyme Road
Hanover, NH 03755-1290

Final Report

Prepared for National Science Foundation
Office of Polar Programs
Antarctic Infrastructure and Logistics
2415 Eisenhower Avenue
Alexandria, VA 22314

Under Engineering for Polar Operations, Logistics, and Research (EPOLAR)
ANT-18-87, "Review and Modeling of Snowdrift Problems at South Pole Station, Antarctica"

Abstract

The elevated building at Scott-Amundsen South Pole Station was designed to mitigate the effects of windblown snow on it and the surrounding infrastructure. Because the elevation of the snow surface increases annually, the station is periodically lifted on its support columns to maintain its design height above the snow surface. To assist with planning these lifts, this effort developed a computational model to simulate snowdrift formation around the elevated building. The model uses computational fluid dynamics methods and synthetic wind record generation derived from statistical analysis of meteorological data. Simulations assessed the impact of several options for the lifting operation on drifts surrounding the elevated building. Simulation results indicate that raising the eastern-most building section (Pod A), or the entire station all at once, can reduce drift accumulation rates over the nearby arches structures. Long-term analyses, spanning 5–6 years, determine whether an equilibrium drift condition may be reached after a long period of undisturbed drift development. These simulations showed that after about 6 years, the rate of growth of the upwind drift slows, appearing to approach an equilibrium condition. However, the adjacent drifts were still increasing in depth at a roughly linear rate, indicating that equilibrium for those drifts was still several seasons away.

Contents

Figures and Tables

Figures

Tables

Preface

This study was conducted for the National Science Foundation (NSF), Office of Polar Programs, Antarctic Infrastructure and Logistics, under Engineering for Polar Operations, Logistics, and Research (EPOLAR), ANT-18-87, "Review and Modeling of Snowdrift Problems at South Pole Station, Antarctica." The technical monitor was Mr. Michael Gencarelli, NSF.

The work was performed by the Engineering Resources Branch (Dr. Melisa Nallar, acting chief) and the Terrestrial and Cryospheric Sciences Branch (Dr. John Weatherly, chief) of the Research and Engineering Division, US Army Engineer Research and Development Center (ERDC), Cold Regions Research and Engineering Laboratory (CRREL). At the time of publication, Dr. Caitlin A. Callaghan was division chief, and Dr. Rosa Affleck was the EPOLAR program manager. The acting deputy director of ERDC-CRREL was Mr. Bryan E. Baker, and the director was Dr. Joseph L. Corriveau.

Thanks to ERDC-CRREL employees Mr. Randal Reynolds and Mr. Jordan Hodges for solids model construction and Mr. Adam LeWinter and Mr. Dominic Filiano for lidar data and expertise.

The simulations were run on the DoD Supercomputing Resource Center's ERDC Onyx and Navy Koehr at their respective High-Performance Computing Centers.

The cover images show (*left*) a view of the windward side and upwind drift for the elevated building and (*right*) the east side and downwind side of the elevated building, showing the drift over the arch structures in the foreground as the structures themselves are buried under the snow.

COL Christian Patterson was commander of ERDC, and Dr. David W. Pittman was the director.

1 Introduction

1.1 Background

The elevated building (Figure 1) at Scott-Amundsen South Pole Station (SPS) is nearing a scheduled incremental lift to reestablish its design elevation over the surrounding snow. Long-term observations of the drifting snow around the elevated building reveal that considerable drifting snow is deposited on the adjacent arch structures that house the garage/shops, power plant, and cargo storage. This unanticipated extra snow overburden on the arches appears to be accelerating the settlement and deformation of these structures, potentially leading to premature failure of these buildings. The National Science Foundation (NSF), who oversees the operations at the US Antarctic facilities, is concerned that lifting the building will exacerbate this issue by depositing more snow on the arches.

The building design allows for a periodic incremental lifting operation to account for the annual increase in bulk snow depth in the region (about 2.76 in.[1] snow water equivalent per year; Fegyveresi et al. 2019). The long-standing plan has been to raise the building all at once. However, NSF was interested if there may be a benefit, such as a reduced drift volume to manage, by lifting the two pods separately.

Figure 1. Illustrations of the elevated building at SPS. To the *left* is an isometric view of the building; on the *right* is a top view.

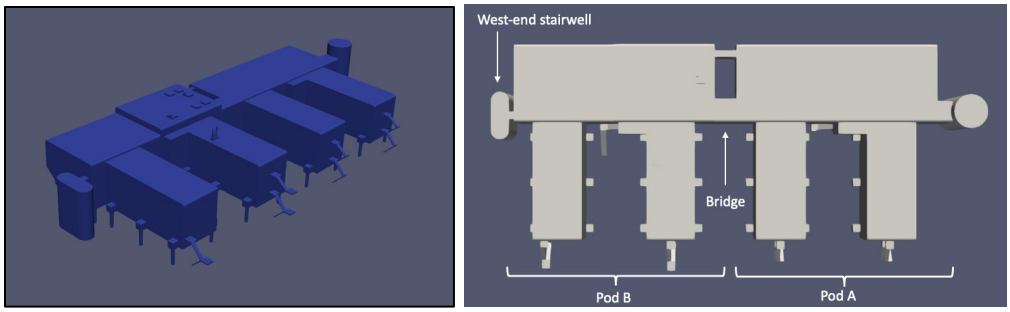

[1] For a full list of the spelled-out forms of the units of measure used in this document and their conversions, please refer to *US Government Publishing Office Style Manual*, 31st ed. (Washington, DC: US Government Publishing Office, 2016), 245–252, https://www.govinfo.gov/content/pkg/GPO-STYLEMANUAL-2016/pdf/GPO-STYLEMANUAL-2016.pdf.

1.2 Objectives

This effort uses computer modeling to consider several scenarios for lifting the elevated station and the potential impact, in terms of snowdrift location and depth, of these different strategies. In contrast to raising the entire elevated building, we considered raising it one pod at a time. Furthermore, we explored the long-term effects of doing no snow removal arounds the elevated building and over the arches for several years to determine how long it may take to achieve an equilibrium drift shape around these buildings and what the resulting drift shape would be. The results of these model studies will inform long-term planning for station management and prioritizing building maintenance.

1.3 Approach

In this paper, we use the SAGE computational flow solver and the particle entrainment, dispersion, and deposition (PEDD) models to investigate snowdrift formation around SPS. SAGE is a general-purpose flow solver developed by the University of Tennessee Space Institute and Flow Analysis, Inc. We chose SAGE for this application due to our extensive experience using SAGE for rotorcraft analysis applications (Steinhoff and Wenren 2006; Wenren, Steinhoff, and Caradonna 2005) as well as related prior work incorporating a predecessor of the PEDD model into SAGE (Haehnel et al. 2008). These models form the computational backbone of our investigation.

Our effort included four main tasks:

Task 1. Conduct statistical analysis of historical meteorological data at the South Pole to determine representative wind directions and speeds for the planned snowdrift simulations. This information is necessary as inputs for the computational model.

Task 2. Prepare solids models of building geometries and initial snow-surface topography as the starting snow surface for the simulations.

Task 3. Conduct simulation of the raising of the SPS elevated building. This includes three subtasks:

   A. Simulate snowdrift accumulation for the elevated building at its current elevation above the existing terrain. This serves as the baseline case to compare the change in drift accumulation for the following subtasks.

B. Simulate the elevated building being lifted one pod at a time to the proposed new height.
C. Simulate the entire elevated building being elevated to its proposed new height.

Task 4. Conduct simulations exploring the potential to achieve an equilibrium drift. This uses the same geometry as in Task 3.A, only the simulation will carry on for multiple seasons to determine what an equilibrium drift shape would look like and how many seasons it would take to reach that state.

Finally, we analyzed the results obtained in Tasks 3 and 4 to determine the relative impact of each scenario on station operations.

2 Wind Record Analysis

2.1 Snow transport

We estimated snow transport by using the procedure of Haehnel and Bigl (2016), which uses an empirical estimation of the instantaneous snow transport, q, as a function of wind speed (Tabler 1994),

$$q\ (\text{lbm s}^{-1}\text{ft}^{-1}) = 0.671\frac{U_{10}^{3.8}}{233846}, \tag{1}$$

where U_{10} is the wind speed at a standard reference height of 32.8 ft (10 m). The parameters used in equation (1) were originally obtained from a fit to Antarctic data (Tabler 1994; Mellor and Fellers 1986). From this equation, we note that the transport depends on nearly the fourth power of the wind speed, meaning that small changes in wind can produce large changes in snow transport. For this reason, the accuracy of the transport prediction strongly relies on the frequency of observations. Infrequent observations with averaging tend to eliminate the peak wind gusts, therefore eliminating the winds that would result in the highest transport. This is also the reason that simply using an average wind speed for the duration of the simulation is not practical as it does not produce significant transport. Fortunately, the meteorological data reported from SPS contains hourly observations; given the relatively high observation frequency, we expect equation (1) to yield reasonable results (Haehnel 2019).

To estimate the cumulative snow transport, Q, for an entire period of interest (e.g., a season or a year) we apply a summation over time, according to the equation

$$Q = \Delta t \sum_{i=1}^{n} q_i, \tag{2}$$

where Δt is the reporting time interval (e.g., hourly) and n is the number of observations over the period of interest (Haehnel and Weatherly 2014). This equation represents the ideal case for which all snow that is picked up from the surface is also deposited somewhere downwind. In reality, a portion of the airborne snow is lost due to sublimation. The fraction of the snow that sublimes away is a function of the distance a snow particle

travels while aloft. Tabler (1994) concludes that any snow that is carried aloft more than 20,000 ft will evaporate before it reaches the ground. He then formulates that the amount of deposited snow, Q_{dep}, is a function of the fetch length, F, as in the equation,

$$Q_{dep} = 0.7Q\left(1 - 0.14^{F/10000\,\text{ft}}\right). \tag{3}$$

Here, the fetch length refers to the unobstructed distance upwind of the region of interest. For sparse locations, such as the South Pole, where the unobstructed distance is functionally infinite, equation (3) reduces to

$$Q_{dep} = 0.7Q. \tag{4}$$

2.2 Wind direction

The starting point for our analysis was an unpublished white paper by Courville et al.,[2] which analyzed meteorological data obtained from the National Oceanic and Atmospheric Administration's Earth System Research Laboratory web repository, spanning 1974–2018. They found that, while the wind direction varied over a wide range, the wind directions that produced significant snow transport were narrowly concentrated between 0° and 30° from grid north. They used the transport equations (1)–(4) to construct wind direction and transport roses for each year. Furthermore, they noted that the majority of the years analyzed had transport prominently centered near 10° east of grid north. This trend is clear in the sample transport roses (representing 2009, 2012, 2015, and 2018) in Figure 2. Based on the observed unimodal transport, we opted to use a fixed wind direction of 10° east of grid north throughout all computational fluid dynamics simulations.

An additional advantage to the fixed-direction inflow model is that it allows us to ignore the effects of snow sintering. Sintering is the phenomenon by which the snowpack hardens and increases in density over time. The effect can be ignored for unvarying wind direction since the deposited

[2] Zoe Courville, Matthew F. Bigl, Dom Filiano, Lynette Barna, Robert B. Haehnel, Jordan Hodge, Yonghu Wenren, Luke D. Allen, and John Gagnon, "Drift Accumulation at the Amundson-Scott South Pole Station" (unpublished white paper, US Army Engineer Research and Development Center, Cold Regions Research and Engineering Laboratory, Hanover, NH, in support of EP-ANT-18-87, "Review and Modeling of Snowdrift Problems at South Pole Station, Antarctica," delivered to the National Science Foundation Antarctic Infrastructure and Logistics Program, 2020).

snow will seldom be reentrained as it will typically be buried by additional drift accumulations.

Figure 2. Snow transport roses at SPS for 2009, 2012, 2015, and 2018. (Image reproduced from Courville et al., "Drift Accumulation.")

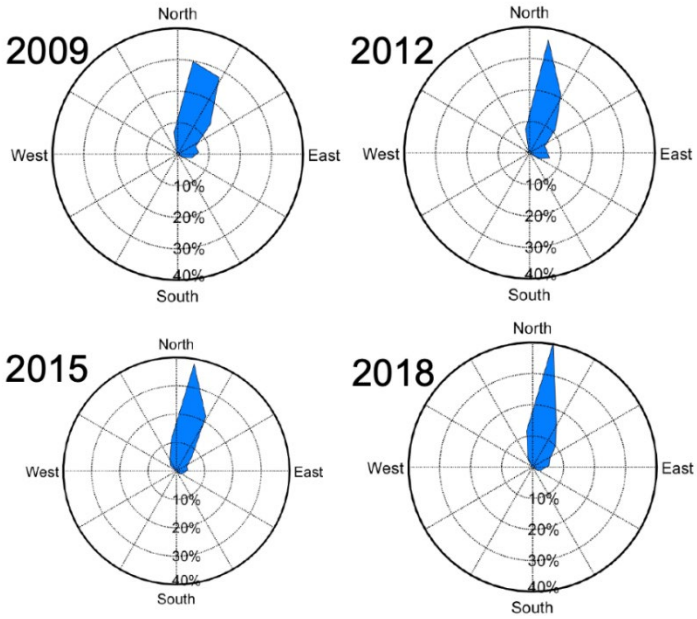

2.3 Composite wind speed model

In addition to knowing the wind direction we required, the SAGE-PEDD model requires a realistic time domain history of the wind speed with lulls and peaks typical of an actual meteorological record. This cannot be accomplished with a cyclic analysis of the period of record for the meteorological data and choosing the daily 95th percentile values; the result of this process gives a nearly sinusoidal record, which is not a realistic meteorological record of wind. Rather than just choose a meteorological record for a year that produced the desired percentile transport, a more robust approach would be to synthesize a wind record that is not any one particular year but is representative of the chosen percentile.

Before generating any synthetic data, we reanalyzed the available meteorological records from 1977 to 2018 (Earth System Research Laboratories 2021). We used equations (1), (2), and (4) to estimate the cumulative transport for each year. Figure 3 shows a histogram summarizing the annual cumulative transport (Q_{dep}) during this period. The distribution was normal except for the outliers. However, we observed that the outliers (especially the high value) could not be safely discarded because they

represent real values and must therefore be considered. With outliers included, the skewness and kurtosis values for the distribution are –0.28 and 1.96, respectively. Because the distribution of annual snow transport cannot be treated as normal, we avoid using parametric descriptions of the data shown in Figure 3 (e.g., mean and standard deviation), opting instead for nonparametric descriptors (e.g., median and percentiles).

Figure 3. Histogram of the annual cumulative snow transport at Amundson-Scott SPS during 1977–2018. The inset shows the calculated 50th, 75th and 95th percentile cumulative transport amounts (lbm = 0.4532 kg, lbm/ft = 0.671 kg/m).

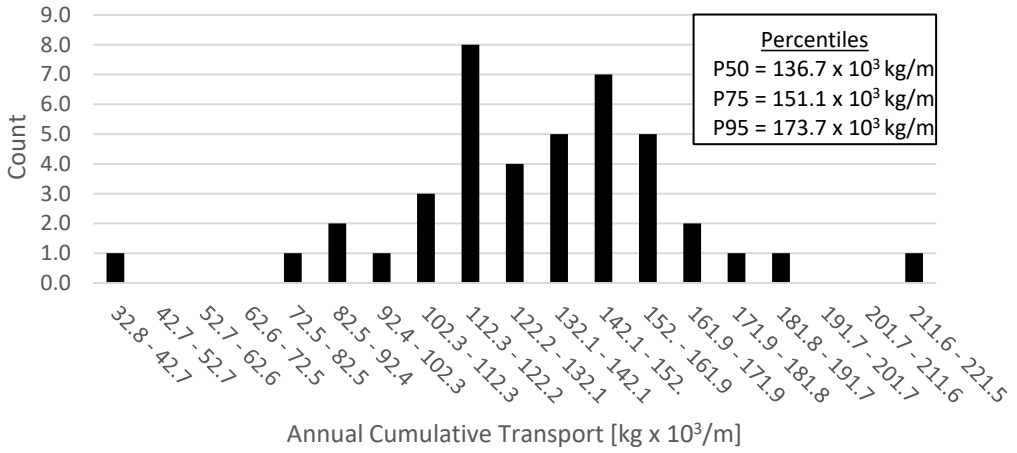

To generate a synthetic wind record, we first select several years to process that are near the target percentile. As stated previously, the goal was to generate wind records corresponding to the 50th and 95th percentiles for snow transport (P50 and P95, respectively). The procedure outlined below uses the P95 case as an example.

The concept was to produce a synthesized wind record that is an approximate average representation of years near the target percentile, in this case the 95th percentile, or P95. We selected 4 years that were close to the P95 transport target: 1981 (P93), 1982 (P86), 1990, (P98), and 2013 (P95). Figure 4 shows the wind speed time series data and probability density functions for these years. Because the distribution of wind data is accurately represented by a Weibull distribution, a fit of this distribution was applied to each of the observed probability density functions in Figure 4 (fit shown as an orange solid line). The Weibull distribution has three parameters that define the shape of the probability density function:

k = shape or Weibull slope.
θ = location.
λ = scale.

Figure 4. Wind speed vs. time (*top*) and wind speed probability density functions (*bottom*) for the 4 years closest to the P95 transport target. The *orange curves* represent curve fits using a Weibull distribution (ft/s = 3.28 m/s).

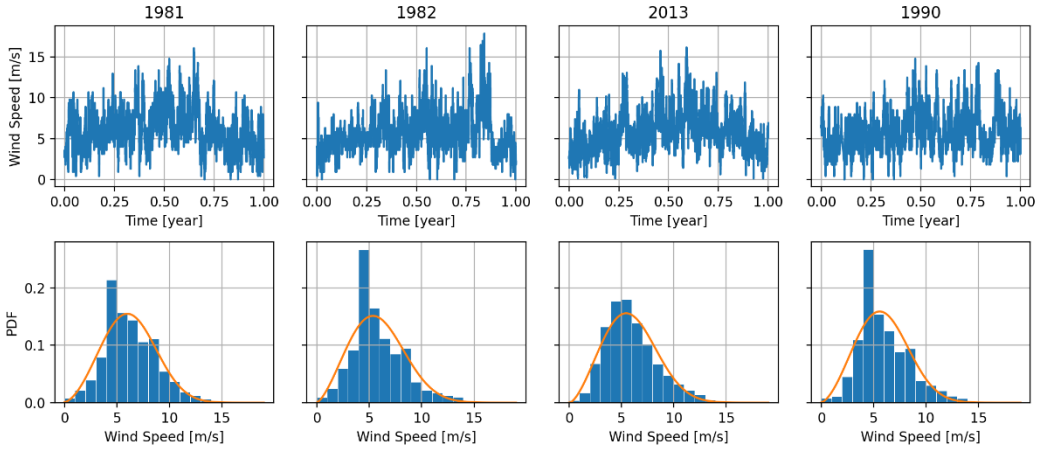

The wind speed record for each year is then converted into the frequency domain using the fast Fourier transform (FFT) algorithm (Cooley and Tukey 1965). The FFT is implemented using

$$\boldsymbol{s} = \mathrm{FFT}(\boldsymbol{v} - \tilde{\boldsymbol{v}}), \tag{5}$$

where

s = the wind speed frequency spectrum,
v = the wind speed in the time domain, and
$\tilde{v}$ = the median wind speed in the time domain.

We subtract the median wind speed value, $\tilde{v}$, to center the resulting spectrum at, or near, zero. Following the transform, the spectra for each year's record are collected into an $m \times n$ table, where m is the number of discrete frequencies in the transform and n is the number of years being collated, as shown in matrix form below:

$$S = \begin{bmatrix} s_{11} & \cdots & s_{1n} \\ \vdots & \ddots & \vdots \\ s_{m1} & \cdots & s_{mn} \end{bmatrix}. \quad (6)$$

The median for each row is then selected to reduce S to the $m \times 1$ vector, $\tilde{s}$, that represents the wind speed FFT of the synthetic year. Because the elements of S are complex numbers, the median cannot be determined directly. Instead, the median is chosen based on the corresponding power spectra, $P(f)$, that is the squared magnitude of the frequency spectra (i.e., $P = |s|^2$). Note that if the number of collated years, n, is even, the lower of the two central elements is used as the median. This "snapping" of the median to an existing value is necessary since taking the average between the elements is meaningless in the complex-number domain.

Finally, we take the inverse FFT (IFFT) of $\tilde{s}$ and reintroduce the median value that was removed in equation (5), yielding a synthetic time-domain wind record, $\hat{v}$, for a typical year:

$$\hat{\boldsymbol{v}} = \mathbf{I}\mathrm{FFT}(\tilde{\boldsymbol{s}}) + \tilde{\boldsymbol{v}}. \quad (7)$$

Wind speed distributions, and thus snow transport values, calculated from $\hat{v}$ are found to closely match the target outcome. For example, the estimated transport for the synthetic or representative P95 year is 115.9 × 10^3 lbm/ft, closely matching the actual value of 116.5 × 10^3 lbm/ft for 2013, the observed P95 year. The fit parameters of the Weibull distribution are similar to those of the individual years from which the record was constructed. Figure 5 and Figure 6 show the synthetic wind speed records and probability density functions for these P50 and P95 cases, respectively. Note that we did not use in the simulations the probability density functions in Figure 5 and Figure 6. We provide plots of them here to verify that the synthetic wind records generated by this method follow the observed distributions at the South Pole. The advantage of this FFT/IFFT approach is that it creates a pseudo-random record while maintaining necessary frequency information that would be lost using other averaging methods. The retained frequency information prevents wild swings in wind speed from one time step to the next and thus simulates correlated phenomenon (lulls or high wind events) that would naturally take place over several hours or days.

Figure 5. Synthetic wind speed record and probability density function (PDF) for the P50 transport year. Note the year 2050 is used to distinguish the synthetic record from actual historical records (ft/s = 3.28 m/s).

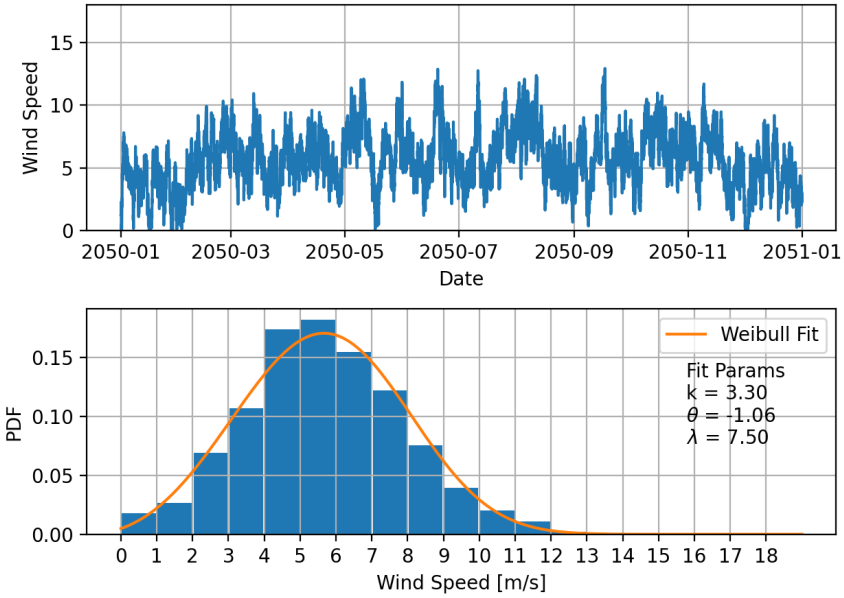

Figure 6. Synthetic wind speed record and probability density function (PDF) for the P95 transport year. Note the year 2050 is used to distinguish the synthetic record from actual historical records (ft/s = 3.28 m/s).

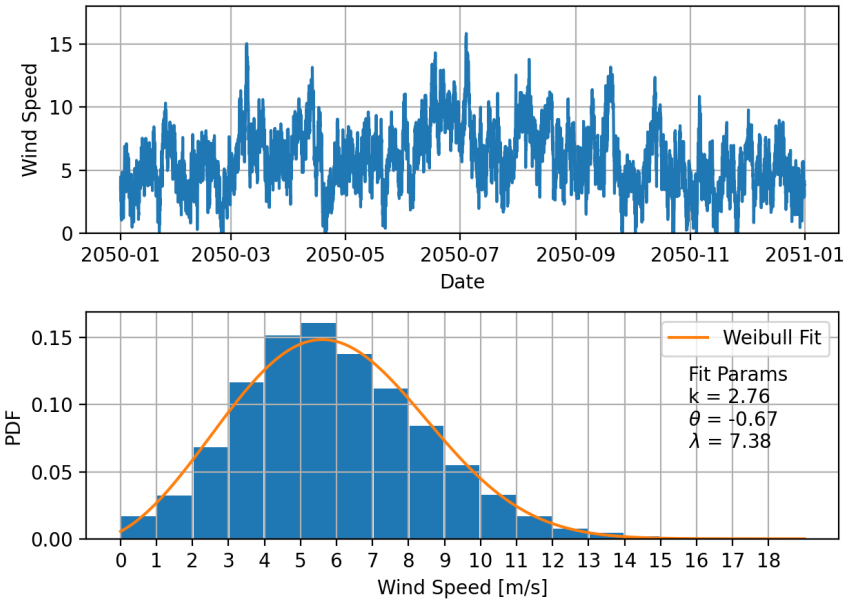

3 Elevated-Building Geometry and Terrain

3.1 Building configurations

The second task dealt with obtaining geometry data and creating geometric models for relevant buildings and the surrounding terrain. We created computer aided design (CAD), or solids, models for the elevated building and arches from as-built drawings supplied by NSF. We then used the building models to simulate the several scenarios outlined in the objectives of this study. Each scenario represents a possible configuration of the elevated building before, during, or after the planned lifting operations. There are four building configurations in total, summarized in Table 1 and visualized in Figure 7. Note that the elevated connector bridge and west-end stairwell (location of these features shown in Figure 1) are removed for configurations requiring the pods of the elevated building to be moved independently—consistent with planning for the operation (M. Gencarelli, NSF planning manager, pers. comm.).

Table 1. Descriptions of the different elevated-building configurations.

Configuration	Description
Baseline	No changes to the current configuration.
A	Pod A is raised by 12.25 ft while pod B remains at its current elevation; bridge and west-end stairwell are removed.
B	Pod B is raised by 12.25 ft while pod A remains at its current elevation; bridge and west-end stairwell are removed.
C	Both pods are raised by 12.25 ft.

Figure 7. Elevated-building configurations shown with start-of-winter snow topography. *Red arrows* point out the absence of the bridge and west-end stairwell in configurations A and B.

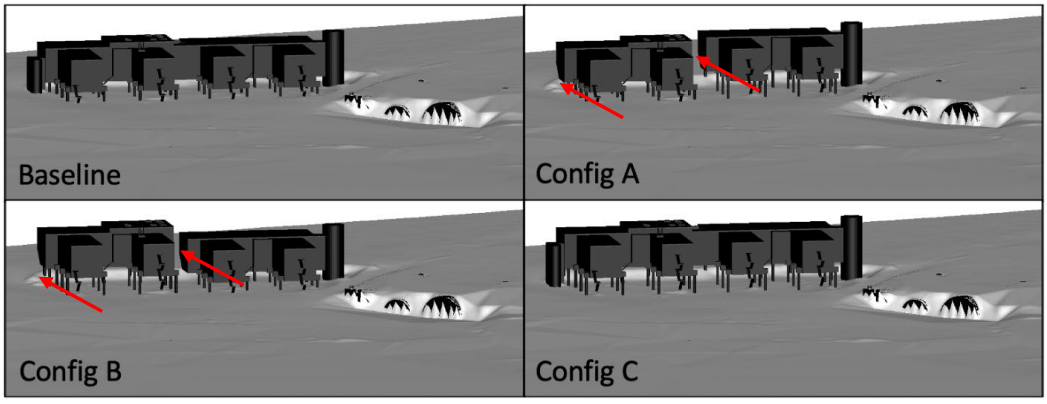

3.2 Initial snow topography

We derived the initial snow topography from survey data from two main sources. The first was a ground survey conducted in 2011, and the second was a lidar survey conducted in 2017:

1. 2011 Ground Survey

   The NSF contractor, Raytheon Polar Services (Skoog and Burnett 2011), conducted this survey on 18–19 November 2011. The survey specifically aimed to assess drift locations and volumes. The data set consists of 388 measured locations surrounding the elevated building and arches. Also, included with the survey data was approximate elevations of the snow surface at the end of the prior summer season. This helped to establish the initial topography immediately around the elevated building and arches before any snowdrifting occurred.

2. 2017 Terrestrial Lidar Survey

   LeWinter et al. (2018) conducted the lidar survey in January 2017 to assess the thermal structure of SPS. Additional work by Courville et al.[3] used the same data to assess the feasibility of using lidar to estimate drift volumes from year to year. This later report points out that, because the survey was not intended to capture the surrounding topography in great detail, many gaps exist in the data. In addition to the notable gaps around the Arches, the extents of the survey are limited to within roughly 230 ft of the raised station. Despite the gaps in the data, the point density of the 2017 survey is substantially higher than that of the 2011 ground survey, with approximately 24 million points making up the snow surface.

It is not possible to use the survey data in its raw form to define the initial snow topography for the SAGE-PEDD flow solver. The data must first be mapped to the nodes of the computational grid. This mapping must accomplish two tasks. First, it must apply spatial transformations (scale factor, rotations, and translations) to bring it into agreement with the SAGE-PEDD coordinate system. Appendix A provides the details of the coordi-

[3] Courville et al., "Drift Accumulation."

nate transformation. For consistency, elevations are converted to feet and given relative to the Naval Civil Engineering Laboratory (NCEL) benchmark established in 1974.

Following coordinate transformation, the irregularly spaced survey points must then be mapped to the regularly spaced SAGE-PEDD computational grid. We wrote a computer program that does this mapping automatically using some user-specified options, the SAGE-PEDD grid file, and the raw survey data. User inputs include

- information about the far-field terrain to enable extrapolation from the edges of the survey data to fill the computational grid and
- manual point entry to fill gaps in the survey (e.g., the region surrounding the entrances to the arches).

Another challenge in defining the initial snow topography is that the survey data sets are from the beginning or middle of the austral summer season. Therefore, drifts from the preceding winter have either not been removed or have been only partially removed. To better approximate the initial condition at the start of the winter season, we implemented a method of levelling the drift topography for each of the major drifts. This was done using cut planes at the same elevations the surveyors in the 2011 survey data used to estimate snowdrift volumes. The two cut planes used were the upwind cut, made at 44.5 ft, and the arches cut, made at 42 ft. Figure 8 shows the locations of each cut plane. Due to the rising snow elevation, the cut planes from 2011 would not be accurate for 2017. To determine the elevation to use for the cut planes for the 2017 data, we added to the 2011 survey's starting snow-surface elevation (i.e., cut planes) the annual far-field snow accumulation of the surrounding plateau: approximately 0.9 ft/year (2.76 in. snow water equivalent cited previously).

Figure 8. Two cut planes were used to reduce the height of prominent drift features. *Contours* are in feet above the 1974 NCEL benchmark.

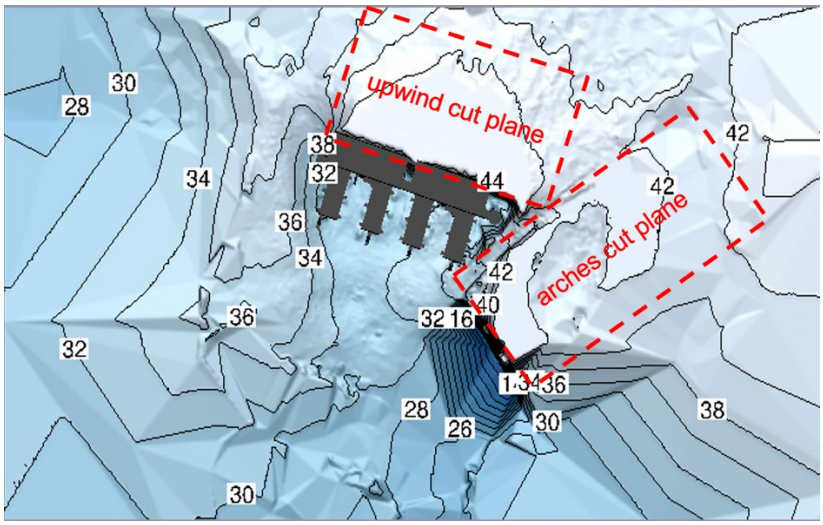

3.3 Drift volume calculation

Drift volume, V, is calculated by subtracting the initial snow surface, ζ_i, from the final snow surface, ζ_f, and integrating over a region of interest, S, as in the equation

$$V = \oiint \left(\zeta_f(S) - \zeta_i(S)\right) dS. \tag{8}$$

The surface integral is approximated using SciPy's implementation of Simpson's Rule (Virtanen et al. 2020; Shklov 1960). The spatial extents of each drift were defined using predetermined polygons drawn on the computational domain. The coordinates may form any nonoverlapping polygon, allowing volume calculations for any size and shape region that may be desired. Four drift regions were identified for this work: the upwind drift, arches drift, arches entrance drift, and west-end drift. Figure 9 shows the boundaries of each drift relative to the elevated building. While the coordinates defining each drift region were somewhat arbitrary, identical coordinates were used for each scenario. This ensures apple-to-apples comparisons between simulated scenarios.

Figure 9. Tracked drifts surrounding the elevated building.

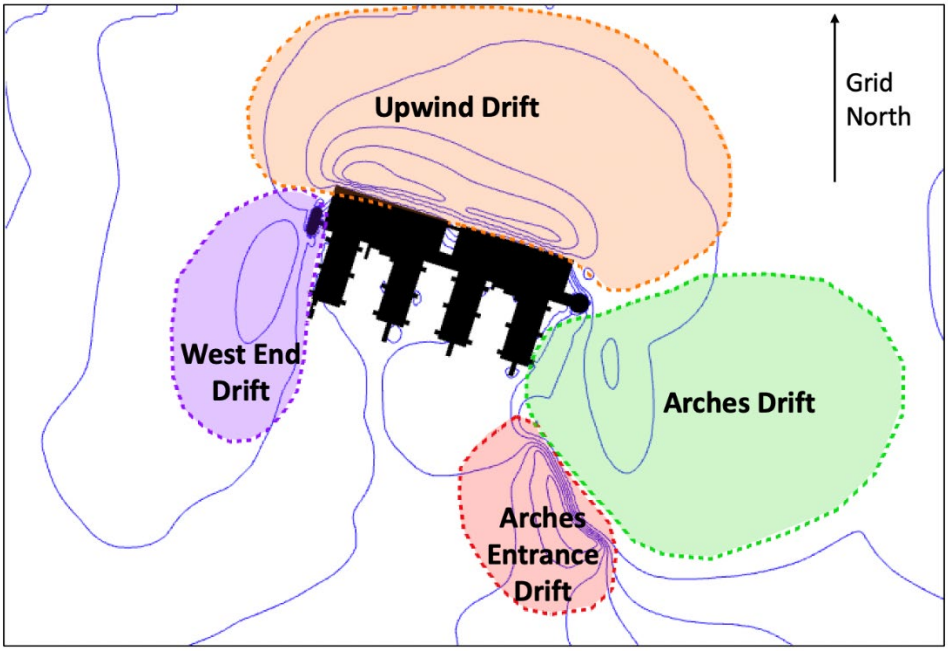

3.4 Scaling time

The numerical time step for a simulation depends on the numerical solution scheme implemented in the flow solver. SAGE-PEDD uses an explicit numerical method, and the computational time-step size is limited. For this work, the maximum stable numerical time step, *dt*, needed to run the simulations is the time within which the snow particles travelling distance equals a 0.2 computational grid cell size. For example, for one case in this work, the grid cell size is 4 ft, and the maximum wind speed is 52 ft/s, *dt* equals 0.01538 s. This work used 222 days (15 February–15 October) as the number of days in a winter season, hence the number of time steps to do an entire simulation is over 1.2 billion. It took approximately 1723.4 compute seconds per time step (using 704 CPUs, that is 2.45 s of wall time per time step). To do a full simulation of one winter season without any adjustments for scaling time, it would take about 93 years to simulate on the US Army Engineer Research and Development Center Onyx High Performance Computing system. To make the run time for these cases reasonable, we implemented the following adjustment to scale time.

We introduce a snow-density scaling factor, ρ_{sc}, a nondimensional value to augment the snow depth for each computational time step (or computational iteration; Haehnel, Wenren, and Allen 2022). The increment in

snow depth, $d\zeta$, added to the existing snow surface in a grid cell adjacent to the ground at each time step is

$$d\zeta = \rho_{sc}\, dx\, \frac{da}{\rho_b}, \tag{9}$$

where

dx = the computational cell size (each is a cube);
da = the change in the suspended snow concentration, a, in the grid cell for that time step; and
ρ_b = the bulk density of the snow on the ground when it is deposited into a drift (typically in the range of 21.8–28.1 lbm/ft^3).

For ρ_{sc} equal to 1, the deposition depth is not augmented (i.e., the increment in snow depth is obtained by compacting the concentration of new suspended snow to a density equal to the bulk density of the snow; we used a ρ_b of 21.8 lbm/ft^3). We consider a ρ_{sc} of 1 a tight coupling between the flow field and the snow deposition rate. Because the computational time steps are small (on the order of 1/100 s), the changes in concentration and snow depth are small for each iteration. The factor ρ_{sc} loosens the coupling between the flow field and snowdrift evolution, allowing the amount of snow deposited to be larger for each computational iteration than changes driven by the flow field would dictate.

The assumption is that amplifying the deposited snow depth by a factor of 10 or 100 will only increase the depth of the snow from around 0.004 in. per time step to 0.04 to 0.4 in. per time step. This small increase in snow depth does not depart significantly from the trend that the drift will take as the simulation progresses or have a gross effect on the flow field; therefore, the flow can be loosely coupled to changes in the deposited drift shape. However, the factor ρ_{sc} cannot be too large or the snowdrifts grow too rapidly for changes in the flow field to stably respond (i.e., the coupling is not tight enough). Yet, if ρ_{sc} is very small, the simulation takes months or years to complete. We have found that this approach is a work in progress; and determining the level of coupling, therefore the value of ρ_{sc}, needs to be adjusted based on computational grid characteristics (grid resolution and domain size). At present, for accurate time scaling, calibration of ρ_{sc} to validation data (e.g., compare the simulated results obtained from

a given model computational grid against snow survey data) gives the most accurate results. Despite the additional time needed for model calibration, this generally is a small price to pay in comparison to the overall savings in computation time.

4 Drift Simulations

4.1 SAGE-PEDD flow solver

SAGE, developed by the University of Tennessee Space Institute and Flow Analysis Inc., is an unsteady-flow solver of the incompressible Euler equations on structured Cartesian grids. SAGE uses the vorticity confinement method to efficiently capture vortices over about two grid cells and the boundary layer flow of objects immersed in the grid. A key element of SAGE is that it efficiently captures the fluctuating vortical structure of the flow, helping to preserve the velocity fluctuations that drive snow transport.

Modeling the effects of particle drag and momentum requires a two-phase (liquid/gas and solid) flow model. SAGE was initially a single-phase model and therefore not capable of simulating particle movement. Haehnel et al. (2008) developed a particle transport model to couple with SAGE to allow modeling of two-phase flow. Their particle entrainment and dispersion (PED) model provided a general-purpose tool for predicting windblown particulates (i.e., dust, which can largely be treated as a passive scalar moving with the flow) from a variety of ground-cover types. Our work modified SAGE and the PED model

- to account for differential velocity between the particles and flow (effects of fluid drag accelerating particle motion),
- to include particle deposition over time scales relevant to drifting snow (e.g., months and years), and
- to introduce inlet boundary condition to simulate a suspended snow concentration profile.

The result of these enhancements is an updated flow solver and the Particle Entrainment, Dispersion, and Deposition (PEDD) model. More information on the SAGE-PEDD model can be found in the *SAGE-PEDD Theory Manual* (Haehnel, Wenren, and Allen 2022).

4.2 Elevated-building lifting scenarios

For the four building configurations described in section 3.1, the final computational grid was identical for all simulations and consisted of approximately 23 million grid cells using a 4 ft grid spacing. Each of the four configurations was simulated using two synthetic wind records, for a total

of eight simulations. The two synthetic wind records were produced to meet the P50 and P95 snow transport targets, respectively, using the methods outlined in section 2. The simulated period was from 15 February through 15 October.

4.3 Equilibrium drift development

A longer simulation was designed to simulate a multiyear scenario in which no snow was removed between seasons. The purpose was to assess whether an equilibrium drift condition could be reached. In this condition, the snow surrounding SPS becomes more streamlined over time, and eventually may reach an equilibrium where no further drift development takes place.

The long-term simulation used the baseline building configuration, and the synthetic wind record for the P95 year was repeated five times. For this case, we used two computational grids. The first used 4 ft grid spacing (identical to lifting-scenario simulations) to better resolve drift detail. The second used a larger 8 ft grid spacing and a larger domain to consider downstream effects. We refer to the two grids as the "fine" and "coarse" grids, respectively. Figure 10 shows the relative size of the two grids. Note that these are two separate grids and are overlayed for comparison only.

Figure 10. Elevated Station computational domains. Contours are in feet above the 1974 NCEL benchmark.

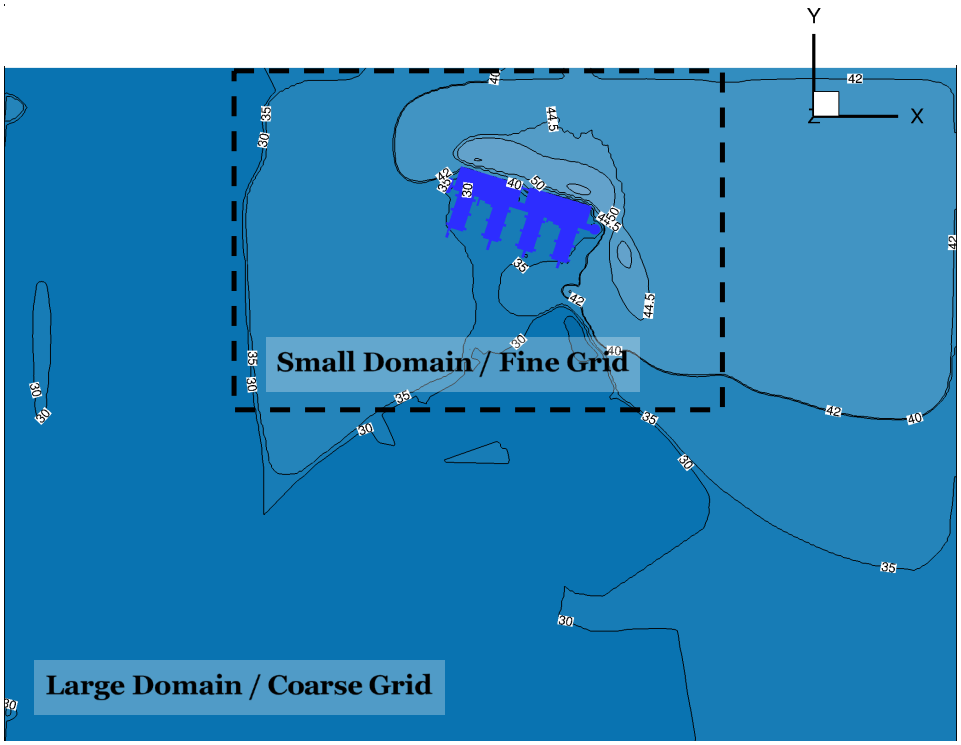

5 Results

5.1 Validation of model drift volumes

Predicted drift volumes were first calculated for the baseline configuration for validation. The calculations from the model were compared to drift volume calculations performed in 2011 (Skoog and Burnett 2011) and 2017.[4] Table 2 shows the results of that comparison. We see that the snowdrift model provides results that are realistic and consistent with field observations. Exact matching of drift volume is difficult as the drift volumes between simulation results and survey data will vary with the extents of the drift region chosen (e.g., polygons selected to integrate the volume as depicted in Figure 9). Furthermore, choosing the correct elevation for the beginning of the winter season—the lower bound for integrating the volume—can be problematic; being off by a foot or more can change the computed volume significantly. The computed volumes use cutting planes, consistent with what is outlined in section 3.2, for establishing a starting topography for the simulation.

These effects may partially explain the simulated upwind drift volume being 40%–70% higher than the observed values (i.e., the polygon we selected in Figure 9 was too large or the starting plane too low). Still, generally, the drift volumes are of the same order of magnitude for the upwind drift; for the arches and west drift the agreement is much better. We note that ρ_{sc} had been calibrated for this baseline case as part of the previous study where this snowdrift model was developed. For a 4 ft grid resolution and the spatial extent used here, a ρ_{sc} of 40 provided good agreement with the observations at the end of a winter season.

We note also that there is little difference in the predicted accumulated drift volume between a P50 and P95 wind record. This may seem surprising at first. However, though more snow may be transported through a region in a given year (more blowing snow for P95 than for P50), the amount of snow deposited around a structure is only a fraction of this (e.g., 25% as suggested by observations in Haehnel and Bigl 2016). Furthermore, the rate of snow deposition is typically nonlinear, with the amount of snow deposited initially being quite high when the buildings are fully exposed to

[4] Dominic L. Filiano, "Amundson-Scott South Pole Station Upwind Drift Volume: Exploration of Techniques Using the 2017 Terrestrial LiDAR" (unpublished report, US Army Engineer Research and Development Center, Cold Regions Research and Engineering Laboratory, Hanover, NH, 2020).

the oncoming wind, and wake regions around the building can be quite large. Over time as the drifts start to build and fill in these wake regions, the combined geometry of drift and building becomes more streamlined, and the rate of drift deposition declines. Therefore, the difference in deposited volume as the overall shape becomes more streamlined may be less profound by the end of the season, even though in early stages the differences can be large.

Table 2. Drift volume comparison with experimental data from 2011 and 2017.

	Upwind Drift Volume (cu. yd)		Arches Drift Volume (cu. yd)		West-End Drift Volume (cu. yd)	
Simulation	P50	P95	P50	P95	P50	P95
Baseline	30089	30222	5961[a]	6164[a]	5748	5711
2011	17630		5382[a]		5495	
2017	21522		28348[b]		N/A	

[a] Volume for snow just over power plant, cargo, and garage arches.

[b] Region used by Filiano in 2020 to compute volume was much larger than in 2011.

5.2 Elevated-building drift simulations

Following validation, we proceeded with the simulations to compare each strategy for raising the building, as described in Table 1. Each simulation used the same computational grid (23 million grid cells) and the same 8-month period. The simulations were performed on the DoD Supercomputing Resource Center's Onyx (Cray XC40/50) and Koehr (HPE SGI 8600) host machines, and each required approximately 240,000 CPU-hours. The total compute time for this phase was roughly 1 million CPU-hours. Using 704 CPUs each, the simulations required approximately 340 hours of wall time to complete.

Table 3 shows the calculated drift volumes for all building configurations and wind conditions, with green cells indicating a reduction in drift volume compared to the baseline (therefore an improved outcome) and red cells highlighting an increase in drift volume. In terms of largest total reduction in drift volume, for the four regions considered, lifting pod A first (configuration A) performs the best with almost a 6% reduction. If the objective is to minimize the accumulation of snow over the arches, lifting the entire station at once (configuration C) is the superior strategy. Configurations B and C have the downside of depositing more snow on the west end of the elevated building; regarding configuration C, the benefit of reducing

the volume over the arches would need to be weighed against increased maintenance associated with a larger snow volume deposited on the west end of the elevated building.

Table 3. Estimated drift volumes following a season of synthetic wind. Baseline drift volumes are given in cubic yards, whereas drift volumes for configurations A, B, and C are given as percent differences from the baseline.

Baseline Volume		Configurations			
		Baseline (yd^3)	A (% Change)	B (% Change)	C (% Change)
Upwind Drift	P50	30089.0	–6.7%	–1.0%	–1.2%
	P95	30221.8	–10.4%	–1.1%	–2.6%
Arches Drift	P50	5961.0	–4.9%	–2.6%	–9.2%
	P95	6164.4	–4.7%	–3.6%	–7.4%
West-End Drift	P50	5747.6	0.3%	5.9%	8.0%
	P95	5711.1	0.5%	9.3%	5.8%
Arches Entrance Drift	P50	15038.9	–0.4%	2.8%	1.2%
	P95	15435.5	–0.2%	2.7%	0.5%
Total Drift	P50	56836.5	–4.2%	0.5%	–0.5%
	P95	57532.8	–5.9%	0.7%	–1.5%

Shading: green = drift volume less than the baseline; red = drift volume greater than the baseline.

5.3 Long-term drift simulation

To accomplish Task 4, we conducted two 5-year simulations of the baseline building configuration. The simulations differed only in their computational grids, as described in 4.3. All other factors (e.g., wind record and duration) were identical. The simulated period represented a considerable computational effort, with simulations running for several weeks to months before completion. The coarse-grid simulation, with fewer grid points, takes less than half the time to complete than the fine grid. Consequently, we could use it to compare our results at the end of one simulated season to the 2011 and 2017 observed snowdrift depths. This allowed us to calibrate the model time scale, via adjustments to ρ_{sc} equals 10, to obtain about the right snow depth at the end of one season as was observed at the end of the 2011 and 2017 winter seasons. This gave us confidence that when the model was run for several seasons, it would give a reasonably accurate estimate of the drift shape for each successive year. Owing to use of a ρ_{sc} of 40 for the 4 ft grid used in the simulations discussed in sections 5.1 and 0, we used that same value for the fine grid with the reduced spatial extent for this case.

Figure 11 shows the snow depths from the fine-grid simulation. The two images are from (A) the end of the first winter and (B) the approximate end of the final winter season, giving a qualitative view of the snowdrift shape surrounding the elevated building and over the arches after several winter seasons.

Figure 11. Snow depth at (*A*) the end of the first winter season and (*B*) the end of the final winter season. Contours are in feet above the 1974 NCEL benchmark.

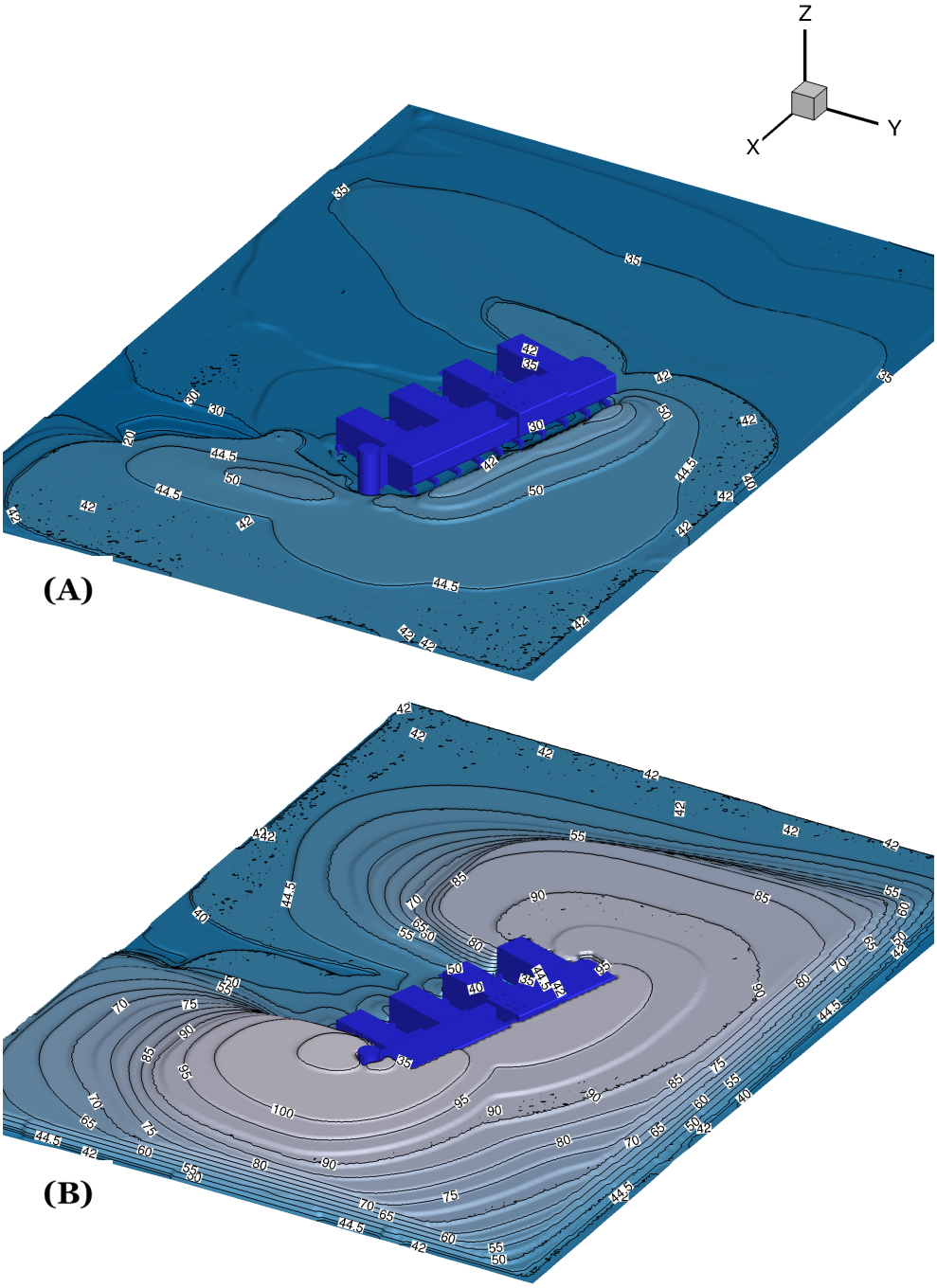

Figure 12 plots the maximum upwind drift elevation throughout both simulations. We see that, for the fine grid, the elevation asymptotically approaches the height of the elevated building. For the coarse grid, we see the drift elevation levels off much earlier. This is likely due to the grid being too coarse to properly resolve the wind, snow, and building interactions. Figure 12 also shows a discrepancy between the snow accumulation rates in the two simulations, with the fine grid predicting about 20%–25% more snow depth at the end of years 1–3 than predicted with the coarse grid. This discrepancy is likely due to the chosen value of 40 for ρ_{sc} being a little too large for the fine-grid case. The change in spatial extents clearly influences the calibration of ρ_{sc} to a computational domain.

Since the snow accumulation rate for the fine-grid case was too high in comparison to the calibrated coarse-grid case, we applied a time dilation factor to the fine-grid simulation results to bring the snow depths into agreement with that of the coarse-grid simulation. Figure 13 shows the adjusted results. When we compensate for the differing accumulation rate, we see that the fine-grid results give estimated snowdrift depths that extend out to approximately the end of a sixth winter season. We also observe that the accumulation rate is decreasing as the drift elevation approaches the top of the building. This indicates that the upwind drift is approaching an equilibrium condition though equilibrium has not been reached after six simulated seasons. We also show that near the end of the third winter season, the simulations predict that the snowdrift just touches the face of the building. We are unsure if this translates to what would actually be observed in the field if the drift was not removed annually—as is the practice—or if this is an artifact of the grid resolution being too coarse to resolve a gap between the drift and upwind face of the building.

We apply the same fine-grid time adjustment factor discussed above to plot the maximum drift elevations of the west-end drift and arches drift, shown in Figure 14 and Figure 15, respectively. From both plots, we see a nearly linear accumulation rate throughout the entire simulation (trend lines shown). The linear trend means that it may still be several more seasons before either drift begins approaching an equilibrium condition.

We expected to see more snow accumulation between, and immediately behind, the downwind extensions, or legs, on the elevated-building pods. We considered that these drifts did not show up due to the coarse-grid resolution used in these simulations (finest grid used was 4 ft grid size). To

explore this effect, we attempted to run a finer grid case (2 ft grid spacing). However, due to the long compute time for the 2 ft grid case, we have not been able to obtain results from that simulation prior to the scheduled timeline to deliver information to NSF on this work. The simulated results for the 2 ft case may be available at a later time.

Figure 12. Maximum upwind drift elevation throughout the 5-year simulated time period. Elevation is relative to the 1974 NCEL benchmark.

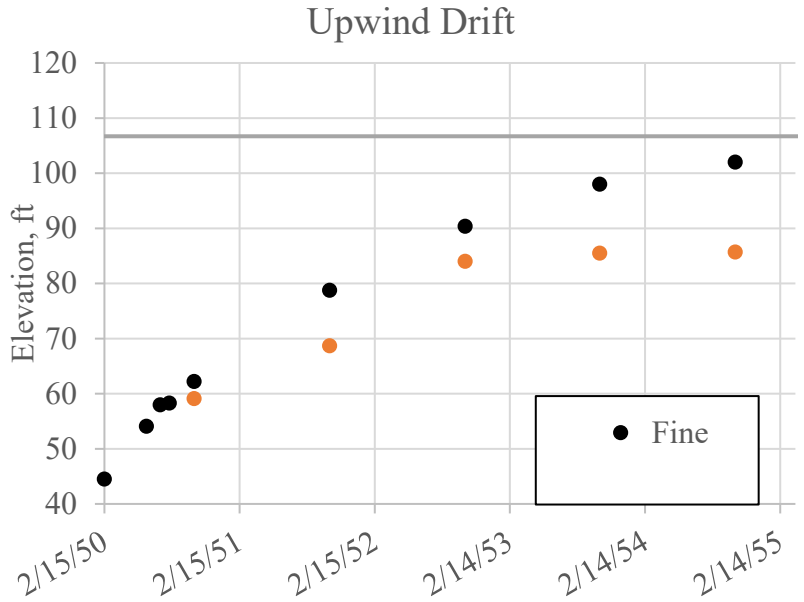

Figure 13. Maximum upwind drift elevation with the accumulation rate of the fine-grid simulation scaled to match the coarse grid. Also shown with the *vertical yellow line* is the approximate time at which the simulation shows that the snow lays against the face of the building. Elevation is relative to the 1974 NCEL benchmark.

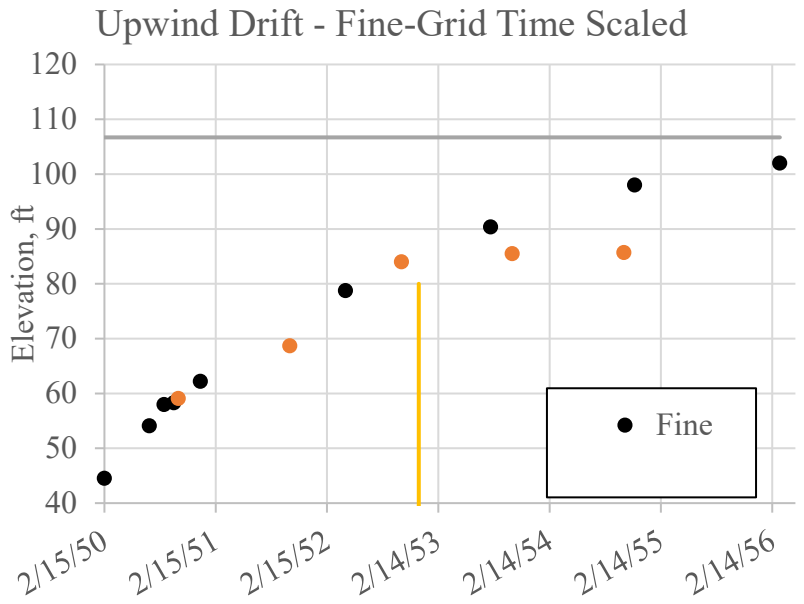

Figure 14. Maximum west-end-drift elevation versus time with a linear trend line. Fine-grid accumulation rate is scaled. Elevation is relative to the 1974 NCEL benchmark.

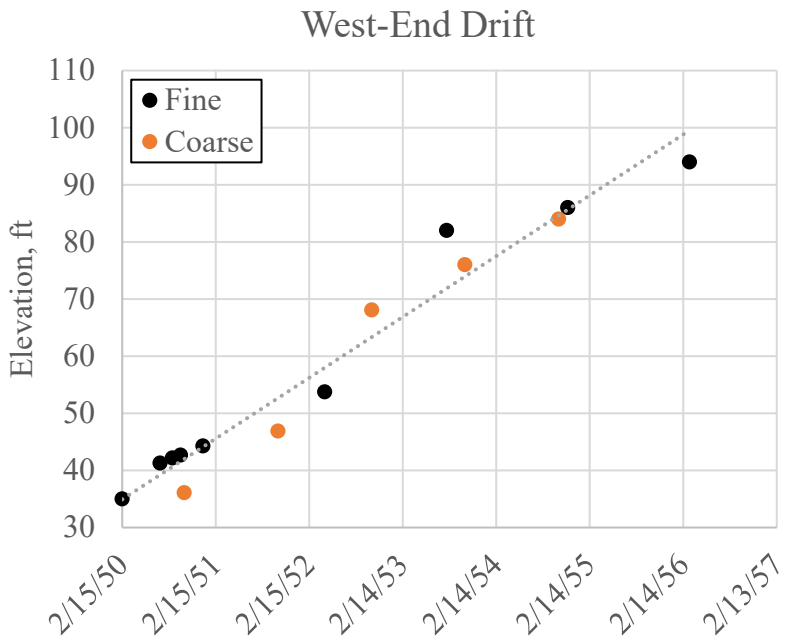

Figure 15. Maximum arches drift elevation versus time with linear trend line. Fine-grid accumulation rate is scaled. Elevation is relative to the 1974 NCEL benchmark.

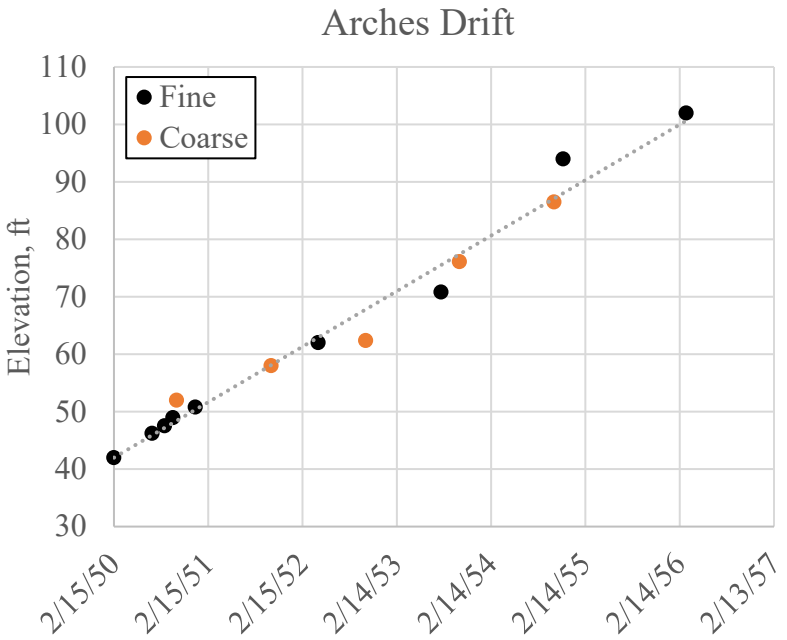

5.4 Computational effort

Here we provide a summary of the amount of compute time required to complete this effort.

Elevated-building drift alternatives

- Computational domain: 23 million grid cells for each simulation (4 ft grid resolution)
- Simulated time: 8 months (15 February–15 October)
- Compute time (per case): 240,000 CPU-hours (340 hr running on 704 CPUs)
- Total compute time: Approx. 1M CPU-hours

Long-term drift case

- Computational domain:
  - Fine grid: 5,896,865 grid points
  - Coarse grid: 2,993,793 grid points
- Simulated time: 5–6 years[5] (1 January 2050–31 December 2054)
- Compute time (per case):
  - Fine grid: 1000 hr (41 days) on 704 CPUs = 704,000 compute hours
  - Coarse grid: 400 hr (17 days) on 704 CPUs = 281,600 compute hours
- Total compute time (4 ft and 8 ft grid only): Approx. 1M CPU-hours

[5] Fine-grid adjusted time

6 Summary and Conclusions

We use the SAGE-PEDD code to simulate several proposed operational scenarios for the SPS elevated building. The simulations were used to explore the resulting drift locations and volumes for each of these scenarios and to guide operational decisions for when and how to raise the elevated building.

To carry out these simulations, we derived a synthetic wind record, that is an approximate average of the wind for several observed seasons, to obtain a representative wind history without relying on a specific year's meteorological record for the simulations. We used the FFT method to decompose the several meteorological records, averaged the frequency and amplitude content, and used IFFT to reconstruct an averaged time-series wind record that preserves the overall snow transport and Weibull distribution characteristics of an actual wind record. This method produces input for the simulation of a representative wind record for a particular snow transport amount that can be considered an average of several seasons rather than picking data from a single season.

We found that in general the snowdrift numerical model provides results that are realistic and consistent with field observations. We summarize below specific conclusions from these simulations.

6.1 Elevated-building lifting simulations

Four simulations considered the effects of different lifting scenarios on snowdrift location and deposited snow volume. The first of these is the baseline case, simulating snowdrift buildup if the elevated building is not lifted from its current height. We compared the results of the other three cases to this baseline case.

The simulations show that lifting the station reduces the total deposited drift volume for all lift scenarios. We also found that the volume of the drift just to the west of the elevated building increases when Pod B is raised (either independently or with entire station). Furthermore, the total drift volume is reduced the most when Pod A is lifted first (by 5%–8%), and the drift volume over arches is reduced the most (5%–9%) when Pod A is raised (either independently or with entire station). Finally, changes

in drift volume for all cases, in comparison to the baseline, is generally less than 10%.

6.2 Long-term drifting simulation

This task explored how many years it may take for an equilibrium drift to form around the elevated building and how large those drifts could be. The main difficulty associated with simulating many seasons is the time it takes to complete the simulation. Even after revising the SAGE-PEDD model and simulations to reduce computation time (section 3.4), it still takes several months to complete, considering total computation time, the time to restart cases, and the time that a submitted job waits in the queue before the computation starts.

For this task, we used a combination of coarser grid (8 ft grid resolution, computational domain has the same extents as used in Task 3) and smaller spatial extents (4 ft grid, same resolution as used in Task 3) to reduce computation time and to explore different aspects. The coarser grid allowed us to consider a larger area that would show how far downwind the snowdrift would extend; the finer grid provided better resolution of the drift shape and gave more detail of the drift geometry around the elevated building. We also used a synthesized wind record that represented the 95th percentile annual snow transport, which should yield a worst-case estimate of drift accumulation (i.e., the quickest time to reach equilibrium).

From these simulations, we found that the upwind drift shows signs of approaching equilibrium (slower rate of growth) after around 5–6 winter seasons. Due to the progressive slowing of the drift accumulation rate, it may be a several more seasons to achieve an equilibrium drift.

We also observed that the drifts' depth near the west stairway and over the arches (east) continues to grow linearly after 5–6 winter seasons. This trend shows that it will take many more seasons for these drifts to reach equilibrium. The slowing drift depth development on upwind drift means incrementally more snow is being delivered to these regions as the upwind drift approaches equilibrium.

6.3 Recommendations

Further model refinements would improve the utility of the SAGE-PEDD. We recommend further study of the relationship between the non-

dimensional time-scaling factor, ρ_{sc}, and the computational grid structure, which would allow selection of the proper value for ρ_{sc} without the need for survey data for calibration. This will allow use of the computational model for new or existing buildings with limited snowdrift-history information.

An ongoing area of model development considers simulating drifting where wind and dominant transport directions vary substantially over the time span of the simulation, such as the bimodal transport histories observed at Summit Station, Greenland.

Owing to the long computational times experienced during this effort, it may be advantageous to explore porting the SAGE-PEDD computer code to be able to run on graphical processing units (GPUs), which are much faster than conventional computer CPUs.

6.4 Conclusions

We developed a general computational model, SAGE-PEDD, that can simulate snowdrift evolution around buildings. In this study, we used the model to determine the effect of several lifting scenarios for the elevated building at the Amundsen-Scott South Pole Station. The results provided a better understanding of short- and long-term effects of different station management strategies. This information was invaluable to the customer, the National Science Foundation, for prioritizing station maintenance efforts for the next 3–5 years.

References

Cooley, James W., and John W. Tukey. 1965. "An Algorithm for the Machine Calculation of Complex Fourier Series." *Mathematics of Computation* 19: 297–301. https://doi.org/10.1090/S0025-5718-1965-0178586-1.

Earth System Research Laboratories. 2021. "GML Data Finder." Global Monitoring Laboratory. Last modified 11 December 2021. https://gml.noaa.gov/dv/data/index.php?parameter_name=Meteorology&site=SPO&frequency=Hourly%2BAverages.

Fegyveresi, John, Tyler J. Fudge, David G. Ferris, Dominic A. Winski, and Richard B. Alley. 2019. *Visual Observations and Stratigraphy of the South Pole Ice Core (SPICEcore): A Preliminary Holocene (~10.2 Ka) Accumulation Record and Depth-Age Chronology*. ERDC/CRREL TR-19-10. Hanover, NH: US Army Engineer Research and Development Center, Cold Regions Research and Engineering Laboratory. http://dx.doi.org/10.21079/11681/33378.

Haehnel, Robert B. 2019 "Blowing Snow Transport Analysis for Estimating Drift Orientation and Severity." Journal of Cold Regions Research and Engineering 33 (2): 05019002. https://doi.org/10.1061/(ASCE)CR.1943-5495.0000184.

Haehnel, Robert B., and Matthew F. Bigl. 2016. *Snow Drift Management: Summit Station Greenland*. Technical Report ERDC/CRREL TR-16-6. Hanover, NH: US Army Engineer Research and Development Center, Cold Regions Research and Engineering Laboratory. http://hdl.handle.net/11681/20337.

Haehnel, Robert B., Marvin A. Moulton, Yonghu Wenren, and John Steinhoff. 2008. "A Model to Simulate Rotorcraft-Induced Brownout." In *Proceedings of the American Helicopter Society 64th Annual Forum*, Montreal, Canada.

Haehnel, Robert B., and John W. Weatherly. 2014. *Antarctic Camps Snow Drift Management Handbook*. ERDC/CRREL TR-14-21. Hanover, NH: US Army Engineer Research and Development Center, Cold Regions Research and Engineering Laboratory. http://hdl.handle.net/11681/5488.

Haehnel, Robert B., Yonghu Wenren, and Luke D. Allen. 2022. *SAGE-PEDD Theory Manual: Modeling Windblown Snow Deposition around Buildings*. ERDC/CRREL TR-22-8. Hanover, NH: US Army Engineer Research and Development Center, Cold Regions Research and Engineering Laboratory. http://dx.doi.org/10.21079/11681/44942.

LeWinter, Adam L., David C. Finnegan, Elias J. Deeb, and Peter J. Gadomski. 2018. *Building Envelope and Infrastructure Assessment Using an Integrated Thermal Imaging and Lidar Scanning System: Amundsen-Scott South Pole Station, Antarctica*. Technical Report TR-18-10. Hanover, NH: US Army Engineer Research and Development Center, Cold Regions Research and Engineering Laboratory. http://dx.doi.org/10.21079/11681/27385.

Mellor, Malcolm, and Gregor Fellers. 1986. "Concentration and Flux of Wind-Blown Snow." Special Report SR 86-11. Hanover, NH: Cold Regions Research and Engineering Laboratory. http://hdl.handle.net/11681/12041.

Shklov, N. 1960. "Simpson's Rule for Unequally Spaced Ordinates." *The American Mathematical Monthly* 67 (10): 1022–23. https://doi.org/10.2307/2309244.

Skoog, K., and T. Burnett. 2011. *Elevated Station Contour Drawing, Sheet No. V-101*. 23 November 2011. Centennial, CO: Raytheon Polar Services.

Steinhoff, John, and Yonghu Wenren. 2006. "An Efficient Vorticity Confinement Based Lifting Surface Method for Rotor Wake Computations." In *Proceedings of the 32nd European Rotorcraft Forum*, Maastricht, Netherlands.

Tabler, R. D. 1994. *Design Guidelines for the Control of Blowing and Drifting Snow*. SHRP-H-318. Washington, DC: National Research Council, Strategic Highway Research Program. https://onlinepubs.trb.org/onlinepubs/shrp/SHRP-H-381.pdf.

Virtanen, Pauli, Ralf Gommers, Travis E. Oliphant, Matt Haberland, Tyler Reddy, David Cournapeau, Evgeni Burovski, et al. 2020. "SciPy 1.0: Fundamental Algorithms for Scientific Computing in Python." *Nature Methods* 17 (3): 261–72. https://doi.org/10.1038/s41592-019-0686-2.

Wenren, Yonghu, J. Steinhoff, and F. Caradonna. 2005. "Application of Vorticity Confinement to Rotorcraft Flows." In *Proceedings of the 31st European Rotorcraft Forum*, Florence, Italy.

Appendix A: Coordinate System Transformation

This section describes the methods for transforming raw survey data to the SAGE-PEDD coordinate system.

Let the SAGE-PEDD and survey coordinate systems be represented by $\mathbb{R}_A$, and $\mathbb{R}_B$, respectively. Additionally, let a denote the vector from the origin to a point in $\mathbb{R}_A$, and b denote the vector from the origin to a point in $\mathbb{R}_B$. The transformation of coordinates is done by selecting two anchor points from each coordinate system, where the anchor points represent the same feature in each system (e.g., the corners of a building). The scale factor, σ, is calculated by

$$\sigma = \frac{\|a_1 - a_2\|}{\|b_1 - b_2\|} \; ; \tag{A-1}$$

and the rotation angle, θ, is calculated by

$$\theta = \cos^{-1}\left(\frac{(a_1 - a_2) \cdot (b_1 - b_2)}{\|a_1 - a_2\|\|b_1 - b_2\|}\right). \tag{A-2}$$

Now we define a vector, b^*, that is the correct magnitude and orientation for b mapped into reference frame A. This is accomplished by multiplying by the scalar σ and then rotating by θ. In matrix form, this equation is

$$b^* = \sigma \begin{bmatrix} \cos\theta & -\sin\theta \\ \sin\theta & \cos\theta \end{bmatrix} \begin{bmatrix} b_x \\ b_y \end{bmatrix}, \tag{A-3}$$

where b_x and b_y are the x and y components of b, respectively. Finally, the translation vector, x, is calculated by

$$x = a_1 - b_1^*. \tag{A-4}$$

Note that the value of x is constant for corresponding points in either reference frame; therefore, x is valid for all points in the survey reference frame. The transformation of any point b into its equivalent position in the SAGE-PEDD reference frame, b', can then be accomplished with

$$b' = \sigma R b + x, \tag{A-5}$$

where R is the two-dimensional rotation matrix as shown in equation (A-3). We note that $\mathbb{R}_A$ is a structured, equally spaced grid while $\mathbb{R}_B$ is an orthographic map projection. For this data set, the projection is Universal Polar Stereographic (UPS): WGS84/UPS South (N, E) using the WGS84 datum with the EGM96 (Global) geoid applied (orthometric heights). Consequently, there may be a small amount of distortion by applying simple translation and rotation. We consider the error in this transformation to be small in comparison to the resolution of the computational grid and, therefore, to have little effect on the simulation.

The final step is to map the points from the transformed survey data to the computational grid. The SAGE flow solver requires a regular grid to operate, whereas survey data is usually provided in an irregular point-cloud format. Furthermore, there is no guarantee that the points from the survey will cover the extents of the computational grid (i.e., the computational grid is larger than the area covered by the survey). These discrepancies are rectified by first mapping the horizontal coordinates of each point onto a regular grid by using linear interpolation and then extending the edges of the surveyed area to the edges of the computational domain by extrapolating to a user-defined, far-field elevation.

We wrote a computer program to accomplish the tasks above. The program takes the SAGE-PEDD grid file (Plot3D format) as an input. Next, it extracts the survey points from a separate file, and transforms their x and y components according to equation (A-5). Now that the points are in the correct frame of reference, the program applies two-dimensional linear interpolation to define the initial snow height, ζ_0, at all locations on the grid that are within the extents of the survey. Finally, it draws a circle with radius, center location, and elevation defined by the user. This circle allows extrapolation of the edge of the surveyed domain outward to cover the computational grid.

Abbreviations

CAD	Computer-Aided Design
CRREL	US Army Cold Regions Research and Engineering Laboratory
ERDC	Engineer Research and Development Center
FFT	Fast Fourier Transform
GPU	Graphical Processing Unit
IFFT	Inverse Fast Fourier Transform
NCEL	Naval Civil Engineering Laboratory
NSF	National Science Foundation
PDF	Probability Density Function
PED	Particle Entrainment and Dispersion
PEDD	Particle Entrainment, Dispersion, and Deposition
SPS	South Pole Station
UPS	Universal Polar Stereographic

REPORT DOCUMENTATION PAGE

Form Approved
OMB No. 0704-0188

1. REPORT DATE (DD-MM-YYYY)	2. REPORT TYPE	3. DATES COVERED (From - To)
August 2022	Technical Report / Final	FY19–FY21

4. TITLE AND SUBTITLE
South Pole Station Snowdrift Model

5a. CONTRACT NUMBER

5b. GRANT NUMBER

5c. PROGRAM ELEMENT

6. AUTHOR(S)
Luke Allen, Robert Haehnel, and Yonghu Wenren

5d. PROJECT NUMBER

5e. TASK NUMBER

5f. WORK UNIT NUMBER

7. PERFORMING ORGANIZATION NAME(S) AND ADDRESS(ES)
US Army Engineer Research and Development Center (ERDC)
Cold Regions Research and Engineering Laboratory (CRREL)
72 Lyme Road
Hanover, NH 03755-1290

8. PERFORMING ORGANIZATION REPORT NUMBER
ERDC/CRREL TR-22-7

9. SPONSORING / MONITORING AGENCY NAME(S) AND ADDRESS(ES)
National Science Foundation
Office of Polar Programs
Antarctic Infrastructure and Logistics
2415 Eisenhower Avenue
Alexandria, VA 22314

10. SPONSOR/MONITOR'S ACRONYM(S)
NSF

11. SPONSOR/MONITOR'S REPORT NUMBER(S)

12. DISTRIBUTION / AVAILABILITY STATEMENT
Approved for public release; distribution is unlimited.

13. SUPPLEMENTARY NOTES
Funded under Engineering for Polar Operations, Logistics, and Research (EPOLAR), ANT-18-87, "Review and Modeling of Snowdrift Problems at South Pole Station, Antarctica"

14. ABSTRACT
The elevated building at Scott-Amundsen South Pole Station was designed to mitigate the effects of windblown snow on it and the surrounding infrastructure. Because the elevation of the snow surface increases annually, the station is periodically lifted on its support columns to maintain its design height above the snow surface. To assist with planning these lifts, this effort developed a computational model to simulate snowdrift formation around the elevated building. The model uses computational fluid dynamics methods and synthetic wind record generation derived from statistical analysis of meteorological data. Simulations assessed the impact of several options for the lifting operation on drifts surrounding the elevated building. Simulation results indicate that raising the eastern-most building section (Pod A), or the entire station all at once, can reduce drift accumulation rates over the nearby arches structures. Long-term analyses, spanning 5–6 years, determine whether an equilibrium drift condition may be reached after a long period of undisturbed drift development. These simulations showed that after about 6 years, the rate of growth of the upwind drift slows, appearing to approach an equilibrium condition. However, the adjacent drifts were still increasing in depth at a roughly linear rate, indicating that equilibrium for those drifts was still several seasons away.

15. SUBJECT TERMS
Amundsen Scott South Pole Station (Antarctica)--Buildings, Computational fluid dynamics, EPOLAR, Foundations--Cold weather conditions, NSF, Snow--Computer simulation, Snow mechanics, Wind forecasting

16. SECURITY CLASSIFICATION OF:			17. LIMITATION OF ABSTRACT	18. NUMBER OF PAGES	19a. NAME OF RESPONSIBLE PERSON
a. REPORT	b. ABSTRACT	c. THIS PAGE			19b. TELEPHONE NUMBER (include area code)
Unclassified	Unclassified	Unclassified	SAR	44	